PERGAMON

International Journal of Heat and Mass Transfer 44 (2001) 4493–4504

International Journal of HEAT and MASS TRANSFER

www.elsevier.com/locate/ijhmt

Multiple solutions for double diffusive convection in a shallow porous cavity with vertical fluxes of heat and mass

L. Kalla [a], M. Mamou [b], P. Vasseur [a,*], L. Robillard [a]

[a] *Department of Mechanical Engineering, Ecole Polytechnique, Campus de l'Universite de Montreal, Case Postale 6079, Succursale A "Centre Ville" Montréal, Québec, Canada H3C 3A7*

[b] *Institute for Aerospace Research, National Research Council Canada, Ottawa, Ontario, Canada K1A DR6*

Received 17 May 2000; received in revised form 16 February 2001

Abstract

The Darcy model with the Boussinesq approximation is used to study double-diffusive natural convection in a shallow porous cavity. The horizontal walls are subject to uniform fluxes of heat and mass, while the side vertical walls are exposed to a constant heat flux of intensity aq', where a is a real number. Results are presented for $-20 \leqslant R_T \leqslant 50$, $-20 \leqslant R_S \leqslant 20$, $5 \leqslant Le \leqslant 10$, $4 \leqslant A \leqslant 8$ and $-0.7 \leqslant a \leqslant 0.7$, where R_T, R_S, Le and A correspond to thermal Rayleigh number, solutal Rayleigh number, Lewis number and aspect ratio of the enclosure, respectively. In the limit of a shallow enclosure ($A \gg 1$) an asymptotic analytical solution for the stream function and temperature and concentration fields is obtained by using a parallel flow assumption in the core region of the cavity and an integral form of the energy and the constituent equations. In the absence of side heating ($a = 0$), the solution takes the form of a standard Bénard bifurcation. The asymmetry brought by the side heating ($a \neq 0$) to the bifurcation is investigated. For high enough Rayleigh numbers, multiple steady states near the threshold of convection are found. These states represent flows in opposite directions. In the range of the governing parameters considered in the present study, a good agreement is observed between the analytical predictions and the numerical simulations of the full governing equations.

1. Introduction

The growing research on double diffusive convection in porous media, where the buoyancy can arise not only from density differences due to variations in temperature but also from those due to variations in solute concentration, is mainly motivated by its importance in many natural and industrial problems. These include drying processes, the transport of a contaminant in saturated soil, the migration of moisture in fibrous insulation, grain storage installations, food processing, etc. Double diffusive flows through porous media are also of interest in geophysical systems, electrochemistry and metallurgy. The state-of-the art has been summarized in a recent book by Nield and Bejan [1].

Early investigations on double diffusive natural convection in porous media primarily focused on the problem of convective instability in a horizontal layer. To this end Nield [2], Taunton et al. [3], Rubin [4], Rudraiah et al. [5], Poulikakos [6], Taslim and Narusawa [7] and Malashetty [8] relied on linear stability analysis to investigate the onset of thermohaline convection in a horizontal porous layer. Criteria for the onset of motion, via stationary and oscillatory modes, were derived by these authors for various conditions. Non-linear stability analyses have also been reported by Rudraiah et al. [5], Brand and Steinberg [9], Nguyen et al. [10] and Mamou et al. [11]. The existence of a subcritical Rayleigh number, at which a convective solution bifurcates from the rest state through finite amplitude convection, was demonstrated in these studies. A combined theoretical and numerical study of

* Corresponding author. Tel.: +1-514-340-4711; fax: +1-514-340-5917.

E-mail address: vasseur@meca.polymtl.ca (P. Vasseur).

0017-9310/01/$ - see front matter
PII: S0017-9310(01)00076-X

List of symbols

A	cavity aspect ratio, L'/H'
a	real number
C_S	constant concentration gradient in x-direction
C_T	constant temperature gradient in x-direction
D	mass diffusivity of species
H'	height of the layer
j'	constant mass flux per unit area
K	permeability of the porous medium
k	thermal conductivity of the fluid saturated porous medium
L'	thickness of the enclosure
Le	Lewis number, α/D
N	buoyancy ratio, $\beta_S \Delta S'/\beta_T \Delta T'$
Nu	Nusselt number, Eq. (10)
q'	constant heat flux per unit area
R_T	thermal Darcy–Rayleigh number, $g\beta_T K H' \Delta T'/\alpha v$
R_S	solutal Rayleigh number, $NLeR_T$
S	dimensionless concentration, $(S' - S'_0)/\Delta S'$
Sh	Sherwood number, Eq. (11)
S'_0	reference concentration at $x' = 0,\ y' = 0$
$\Delta S'$	characteristic concentration, $j'H'/D$
ΔS	dimensionless wall-to-wall concentration difference
T	dimensionless temperature, $(T' - T'_0)/\Delta T'$
t	dimensionless time, $t'\alpha/\sigma H'^2$
T'_0	reference temperature at $x' = 0,\ y' = 0$
$\Delta T'$	characteristic temperature, $q'H'/k$
ΔT	dimensionless wall-to-wall temperature difference
u	dimensionless velocity in x-direction, $u'H'/\alpha$
v	dimensionless velocity in y-direction, $v'H'/\alpha$
x	dimensionless coordinate axis, x'/H'
y	dimensionless coordinate axis, y'/H'

Greek symbols

α	thermal diffusivity, $k/(\rho C)_f$
β_S	concentration expansion coefficient
β_T	thermal expansion coefficient
ε	normalized porosity of the porous medium, ϕ/σ
v	kinematic viscosity of the fluid
μ	dynamic viscosity of the fluid
θ_S	dimensionless concentration field, Eq. (14)
θ_T	dimensionless temperature field, Eq. (13)
ρ	density of the fluid
$(\rho C)_f$	heat capacity of fluid
$(\rho C)_p$	heat capacity of saturated porous medium
σ	heat capacity ratio $(\rho C)_p/(\rho C)_f$
ϕ	porosity of the porous medium
Ψ	dimensionless stream function, Ψ'/α
Ψ_c	stream function value at the center of the enclosure, Eq. (25)

Superscripts

$'$	dimensional variable
sub	subcritical
sup	supercritical

Subscripts

c	onset of motion; or center of the cavity
max	maximum value
min	minimum value
$\circ$	reference state

the mass transfer effected by high Rayleigh number Bénard convection in a two-dimensional saturated porous layer heated from below was conducted by Trevisan an Bejan [12]. Three distinct scaling laws were proposed to predict the overall mass transfer rate in terms of the Rayleigh and Lewis numbers. Convective flows through porous media heated from below in a square domain with two opposing sources of buoyancy have been investigated numerically by Rosenberg and Spera [13] for a variety of boundary and initial conditions on the salinity field. Steady-state calculations of porous media heated and salted from below were obtained by these authors in order to predict the effect of the Rayleigh and Lewis numbers and buoyancy ratio on both Nusselt and Sherwood numbers. Double diffusive fingering convection in a horizontal porous medium in which it was assumed that the flow exhibits a horizontal periodicity has been studied by Chen and Chen [14]. The stability boundaries which separate regions of different types of convective motion were identified in terms of the thermal and solute Rayleigh numbers.

All the above studies are concerned with the onset and development of double diffusive convective flows within a porous material subject to vertical destabilizing density gradients induced by the presence of two-components in the fluid, with different diffusivities. In particular, this type of situation has been considered by Mamou et al. [11] for the case of a shallow horizontal porous cavity with constant fluxes of heat and mass applied on the two opposing horizontal sides while the vertical boundaries are kept impermeable and adiabatic. Analytical solutions were obtained for the flow, temperature and solute fields using a parallel flow approximation. In particular, the bifurcation diagrams for the onset of unicellular convective motion were demonstrated to be perfectly symmetrical. Also the critical Rayleigh numbers for onset of supercritical and

subcritical convection flows were predicted analytically.

In the present investigation, the effects of a weak horizontal temperature gradient on the convective flow induced in a porous layer heated and salted from below are investigated. It will be shown that this parameter alters the symmetry properties of the bifurcation diagrams mentioned above. The study is also concerned with the possible existence of multiple steady-state solutions for a given set of the governing parameters. The first part of the paper presents an analytical approach to the development of the convective flow using a parallel flow approximation. The second part presents numerical results for the flow field, temperature and concentration distributions, and heat and mass transfer rates for various flow regimes. The fully non-linear set of governing equations is solved numerically using a finite difference method with an implicit scheme.

2. Formulation of the problem

The geometry of the problem is shown in Fig. 1. The shallow horizontal porous enclosure is of height H' and thickness L', and the Cartesian coordinates (x', y') with the corresponding velocity components (u', v') are indicated herein. The top and bottom horizontal boundaries are subject to vertical uniform fluxes of heat and mass per unit area, q' and j', respectively. A uniform heat flux aq', is applied on the two vertical impermeable walls. The porous matrix is assumed to be homogenous and isotropic and the appropriate Darcy model is used. Interaction between the thermal and concentration gradients, known as Soret and Dufour effects, are neglected. The fluid that saturates the porous matrix is modeled as a Boussinesq fluid whose density, ρ, varies linearly with temperature T' and concentration S' as

$$\rho = \rho_0\left[1 - \beta_T(T' - T'_0) - \beta_S(S' - S'_0)\right], \tag{1}$$

where ρ_0 is the fluid density at temperature T'_0 and concentration S'_0, and β_T and β_S are the thermal and concentration expansion coefficients, respectively. The subscript 0 refers to conditions at the origin of the coordinate system.

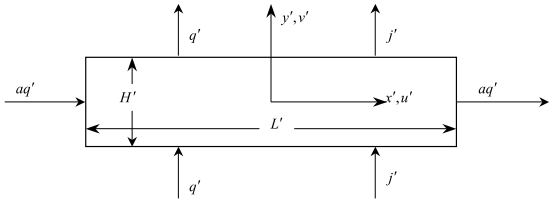

Fig. 1. Flow configuration and coordinate system.

The following dimensionless variables are used

$$\begin{aligned}&(x,y) = (x',y')/H', \quad (u,v) = (u',v')H'/\alpha, \quad t = t'\alpha/H'^2\sigma,\\ &T = (T' - T'_0)/\Delta T', \quad S = (S' - S'_0)/\Delta S', \quad \Delta T' = q'H'/k,\\ &\Delta S' = j'H'/D, \quad \varepsilon = \phi/\sigma,\end{aligned} \tag{2}$$

where t' is the time, k and D the thermal conductivity of the saturated porous medium and the mass averaged diffusivity through the fluid mixture, respectively, $\alpha = k/(\rho C)_f$, the thermal diffusivity of the porous medium, $\sigma = (\rho C)_p/(\rho C)_f$, the saturated porous medium to fluid heat capacity ratio, and ϕ is the porosity of the porous matrix.

In the following analysis, the stream function formulation is introduced in the mathematical model. In order to satisfy the continuity equation, the stream function Ψ is defined such that

$$u = \frac{\partial \Psi}{\partial y}, \quad v = -\frac{\partial \Psi}{\partial x}. \tag{3}$$

In terms of the above definitions, the dimensionless governing equations expressing conservation of momentum, energy and species are, respectively,

$$\nabla^2 \Psi = -R_T \frac{\partial}{\partial x}(T + NS), \tag{4}$$

$$\nabla^2 T = u\frac{\partial T}{\partial x} + v\frac{\partial T}{\partial y} + \frac{\partial T}{\partial t}, \tag{5}$$

$$\frac{1}{Le}\nabla^2 S = u\frac{\partial S}{\partial x} + v\frac{\partial S}{\partial y} + \varepsilon\frac{\partial S}{\partial t}. \tag{6}$$

The dimensionless boundary conditions sketched in Fig. 1 are

$$x = \pm\frac{A}{2}, \quad \Psi = 0, \quad \frac{\partial T}{\partial x} = -a, \quad \frac{\partial S}{\partial x} = 0, \tag{7a}$$

$$y = \pm\frac{1}{2}, \quad \Psi = 0, \quad \frac{\partial T}{\partial y} = -1, \quad \frac{\partial S}{\partial y} = -1. \tag{7b}$$

Eqs. (4)–(6), (7a), (7b) indicate that the present problem is governed by the following dimensionless parameters, namely the thermal Darcy–Rayleigh number R_T, the solutal to buoyancy ratio N, the Lewis number Le, the cavity aspect ratio A and the normalized porosity ε defined as

$$\begin{aligned}&R_T = \frac{g\beta_T K\Delta T' H'}{\alpha\nu}, \quad N = \frac{\beta_S \Delta S'}{\beta_T \Delta T'},\\ &A = L'/H', \quad Le = \alpha/D, \quad \varepsilon = \phi/\sigma,\end{aligned} \tag{8}$$

where K is the permeability of the porous medium, g the acceleration due to gravity and ν the kinematic viscosity of the fluid.

Naturally, the solution of the present problem depends also on the magnitude of the heat flux imposed on the vertical walls of the cavity, i.e. on the value of the parameter a.

3. Numerical solution

A finite difference method was used to obtain numerical solutions of the complete governing Eqs. (4)–(6). The equations for the stream function, Eq. (4), and temperature and concentration, Eqs. (5) and (6) are first discretized according to the well-known central difference scheme for a regular mesh size. The discretized equations for Ψ, T and S are then solved at each time step using the last available field values, until convergence to a steady or to a stationary oscillation state is achieved.

The energy and concentration equations (5) and (6) were solved using an alternating direction implicit (ADI) method. The stream function field was obtained from Eq. (4) using the successive over-relaxation (SOR) method and known temperature and concentration distributions. The iterative procedure was repeated until the following condition was satisfied:

$$\frac{\sum_i \sum_j \left| \Psi_{i,j}^{n+1} - \Psi_{i,j}^{n} \right|}{\sum_i \sum_j \left| \Psi_{i,j}^{n+1} \right|} \leqslant 10^{-4}, \tag{9}$$

where the superscripts indicate the value of the nth and $(n+1)$th iterations, respectively, the subscript i and j indices denote grid locations in the (x, y) plane. A further decrease of the convergence criteria 10^{-4} did not cause any significant change in the final results.

The accuracy of the numerical model was verified by comparing results from the present investigation with several results in literature. Since the validation of the present code has already been discussed in the past by Mamou et al. [11], the details will not be presented here. Naturally, the precision of the numerical results depends on the mesh size, which is a function of the governing parameters and particularly of the aspect ratio of the cavity. Most of the numerical results presented here were obtained for $A = 4$ for which a mesh of 100×60 was found sufficient to model accurately the problem. However, when an aspect ratio $A = 8$ was necessary to describe the parallel flow pattern, a mesh size of 280×80 was used.

In the present notation, the Nusselt and Sherwood numbers in the vertical direction, are given, respectively, by

$$Nu = \frac{q'}{k\overline{\Delta T'}/H'} = \frac{1}{\Delta T} \tag{10}$$

and

$$Sh = \frac{j'}{D\overline{\Delta S'}/H'} = \frac{1}{\Delta S}, \tag{11}$$

where $\overline{\Delta T'} = T'(0,-1/2) - T'(0,1/2)$ and $\overline{\Delta S'} = S'(0,-1/2) - S'(0,1/2)$ are the temperature and concentration differences between the lower and upper walls of the enclosure at the position $x = 0$.

4. Analytical solution

For sufficiently large aspect ratios A, the present problem can be significantly simplified by the parallel flow approximation. The analytical procedure used here has been presented before (see for instance [11,15,16] so that only a brief outline will be included before passing on to the results obtained from it. In the central part of the layer, the flow velocity can be assumed to be parallel in the x-direction, such that only the velocity component $u(y)$ in that direction exists. Thus, it is assumed that

$$\Psi(x, y) \approx \Psi(y). \tag{12}$$

Also, the temperature and concentration fields are the sums of a linearly varying longitudinal part and an unknown transverse distribution so that

$$T(x, y) = C_{\mathrm{T}} x + \theta_{\mathrm{T}}(y) \tag{13}$$

and

$$S(x, y) = C_{\mathrm{S}} x + \theta_{\mathrm{S}}(y), \tag{14}$$

where C_{T} and C_{S} are unknown constant temperature and concentration gradients, respectively, in the x-direction. Substituting in the governing equation (4) and in the steady form of Eqs. (5) and (6), we obtain

$$\frac{\mathrm{d}^2\Psi}{\mathrm{d}y^2} = -R_{\mathrm{T}}(C_{\mathrm{T}} + NC_{\mathrm{S}}), \tag{15}$$

$$\frac{\mathrm{d}^2\theta_{\mathrm{T}}}{\mathrm{d}y^2} = C_{\mathrm{T}} \frac{\mathrm{d}\Psi}{\mathrm{d}y}, \tag{16}$$

$$\frac{\mathrm{d}^2\theta_{\mathrm{S}}}{\mathrm{d}y^2} = Le\, C_{\mathrm{S}} \frac{\mathrm{d}\Psi}{\mathrm{d}y}. \tag{17}$$

Boundary conditions in the y direction are now

$$y = \pm\frac{1}{2}: \quad \Psi = 0, \qquad \frac{\partial\theta_{\mathrm{T}}}{\partial y} = -1, \quad \frac{\partial\theta_{\mathrm{S}}}{\partial y} = -1. \tag{18}$$

The thermal and solutal boundary conditions in the x-direction cannot be reproduced exactly with the parallel flow approximation. Instead, following Trevisan and Bejan [15], it can be easily demonstrated that the heat and solute transports across a transversal section, at any x, are given by the following expressions:

$$\int_{-1/2}^{1/2} Tu\,\mathrm{d}y - \int_{-1/2}^{1/2} \frac{\partial T}{\partial x}\,\mathrm{d}y = a \tag{19}$$

and

$$\int_{-1/2}^{1/2} Su\,\mathrm{d}y - \frac{1}{Le}\int_{-1/2}^{1/2} \frac{\partial S}{\partial x}\,\mathrm{d}y = 0. \tag{20}$$

Solutions of Eqs. (15)–(17) satisfying the boundary conditions (18) are:

$$\Psi = -\Psi_c(4y^2 - 1), \tag{21}$$

$$u = -8\Psi_c y, \tag{22}$$

$$T = C_T x - \frac{C_T \Psi_c}{3}(4y^3 - 3y) - y, \tag{23}$$

$$S = C_S x - \frac{C_S Le\,\Psi_c}{3}(4y^3 - 3y) - y, \tag{24}$$

where

$$\Psi_c = \frac{3}{2}R_T^0(C_T + NC_S) \tag{25}$$

and

$$R_T^0 = \frac{R_T}{R^{sup}} \quad \text{with } R^{sup} = 12. \tag{26}$$

Substituting Eqs. (21)–(26) into Eqs. (19) and (20) yields the following expressions for C_T and C_S:

$$C_T = \frac{(4\Psi_c - 6a)b}{3(2b + \Psi_c^2)} \tag{27}$$

and

$$C_S = \frac{4b\,Le\,\Psi_c}{3(2b + Le^2\Psi_c^2)}, \tag{28}$$

where $b = 15/16$.

Substituting Eqs. (27) and (28) into Eq. (25) yields the following expression for Ψ_c:

$$\sum_{i=0}^{5} a_i \Psi_c^i = 0, \tag{29}$$

where

$$\begin{aligned} a_0 &= 6b^2 R_T^0 a,\\ a_1 &= -4b^2\left[R_T^0(1 + N\,Le) - 1\right],\\ a_2 &= 3ab\,Le^2\,R_T^0,\\ a_3 &= -2b\left[R_T^0 Le(N + Le) - (1 + Le^2)\right],\\ a_4 &= 0,\\ a_5 &= Le^2. \end{aligned} \tag{30}$$

The x-temperature gradient C_T and solutal gradient C_S in the stream function and temperature and concentration field solutions, Eqs. (21), (23) and (24), can be obtained for any combination of the controlling parameters R_T, N, Le and a by numerically solving the transcendental equations (29) and (30).

Substituting Eqs. (23) and (24) into Eqs. (10) and (11), it is found that the Nusselt and Sherwood numbers are given, respectively, by

$$Nu = \frac{6(\Psi_c^2 + 2b)}{(12b + \Psi_c^2)} \tag{31}$$

and

$$Sh = \frac{6(2b + Le^2\Psi_c^2)}{(12b + Le^2\Psi_c^2)}. \tag{32}$$

5. Results and discussion

The analytical solution obtained from the parallel flow approximation was compared against the numerical solution obtained with a finite difference program based on the numerical approach described early. Comparison of the analytical and numerical results is presented in this section.

As discussed earlier, the present problem is governed by six dimensionless parameters, namely R_T, N, Le, A, ε and a. In the following discussion, it is assumed that the normalized porosity of the porous medium is $\varepsilon = 1$. Also, the analytical solution is obtained on the basis of the shallow cavity approximation ($A \gg 1$) such that the results predicted by this model are more accurate at large A.

5.1. Convection in the absence of side heating ($a = 0$)

Double-diffusive convection in a horizontal porous layer induced solely by vertical gradients of heat and solute will be discussed first. Typical bifurcation diagrams will be presented for the case when the temperature gradient is destabilizing and when the concentration gradient is either stabilizing or destabilizing. Then the effect of side heating on these bifurcation diagrams will be investigated.

For finite amplitude convection, the velocity, temperature and concentration fields and Nusselt and Sherwood numbers are obtained from Eqs. (21), (23), (24), (31) and (32), where the value of C_T, C_S and Ψ_c are evaluated by setting $a = 0$ into Eqs. (27)–(30).

From Eqs. (29) and (30), it is readily found that the flow intensity Ψ_c is given by

$$\Psi_c = \pm\frac{\sqrt{b}}{Le}\left[d_1 \pm \sqrt{d_1^2 + d_2^2}\right]^{1/2}, \tag{33}$$

where

$$\begin{aligned} d_1 &= R_T^0 Le(N + Le) - (Le^2 + 1),\\ d_2 &= 4Le^2[R_T^0(1 + N\,Le) - 1]. \end{aligned} \tag{34}$$

The above results are in agreement with those predicted in the past by Mamou et al. [11] while studying

double-diffusive convection in a horizontal porous layer heated and salted from below.

From the above equations, it is seen that five steady-state solutions are possible. One corresponds to the rest state regime ($\Psi_c = 0$) and the four others to finite amplitude flow regimes. The signs + and − outside the brackets refer to the possible occurrence of counter-clockwise and clockwise circulations, respectively. Inside the brackets, they refer to stable and unstable branches, respectively.

The onset of supercritical convection R_{Tc}^{sup}, characterized by a transition from the quiescent state to convective regime occurring through zero flow amplitude ($\Psi_c = 0$), is obtained when the conditions $d_1 < 0$ and $d_2 = 0$ are satisfied, as

$$R_{Tc}^{sup} = 12 - R_S, \tag{35}$$

where subscript c refers to the onset of motion, subscript sup to supercritical Rayleigh number, $R_S = R_T N Le$ being the solutal Rayleigh number.

Another type of onset of motion, characterized by a transition from the rest state through a finite amplitude convection $\Psi_c = \sqrt{bd_1}/Le$, is also possible. The threshold for this latter, called subcritical bifurcation, occurs only when the buoyancy forces induced by the thermal and solutal contributions are opposing each other. The subcritical Rayleigh number Ra_{Tc}^{sub} at which such flows are induced can be obtained from the conditions $d_1 > 0$ and $d_1^2 + d_2 = 0$, as

$$Ra_{Tc}^{sub} = \frac{12}{Le^2}\left(\sqrt{Le^2 - 1} + \sqrt{-R_S/12}\right)^2. \tag{36}$$

Fig. 2(a) shows the bifurcation diagram for Ψ_c as a function of thermal Rayleigh number R_T, in the case of pure thermal convection ($R_S = 0$). This situation corresponds to the classical Bénard problem. A pitchfork bifurcation occurs at a critical Rayleigh number

$$R_{Tc}^{sup} = 12 \tag{37}$$

as given by Eq. (33). This critical Rayleigh number has been predicted in the past by Nield [2] on the basis of the linear stability theory. The prediction of the onset of motion is correctly deduced from a parallel flow approximation due to the fact that the onset of motion within a horizontal layer heated from below by a constant heat flux occurs at zero wave number. The analytical solution, represented by a line, is seen to be in excellent agreement with the numerical solution of full governing equations, depicted by black dots.

Figs. 2(b) and (c) summarize the ways in which the pitchfork bifurcation diagram for pure thermal convection (Fig. 2(a)) is affected by the presence of a solutal contribution when $Le = 10$. Fig. 2(b) exemplifies the bifurcation diagram for the case $R_S = 10$ for which both the thermal and solutal contributions are destabilizing. The occurrence of two distinct convective regimes is observed. For R_T between the thermal–solutal and the thermal thresholds, Eqs. (33) and (35), respectively, a weak convective flow exists. This type of flow is illustrated in Fig. 3(a) which shows streamlines and contours of temperature, concentration and density for the case $R_T = 5$. The approximate validity of the parallel flow approximation in the central region of the cavity is evident. The contributions of temperature and concentra-

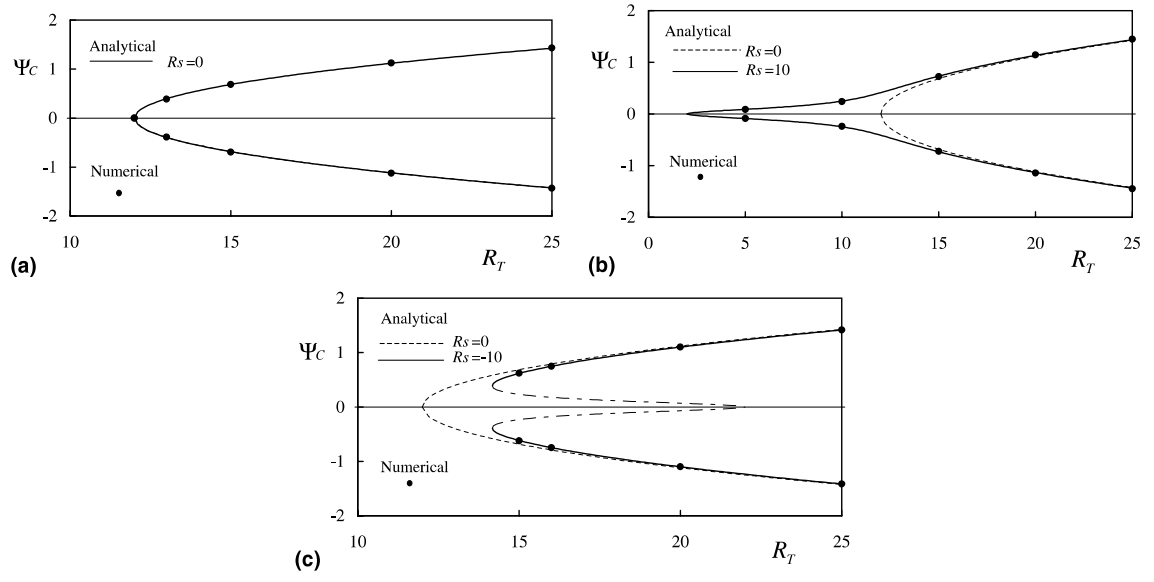

Fig. 2. Bifurcation diagrams for $Le = 10$: (a) $R_S = 0$, pure thermal convection; (b) $R_S = 10$, a destabilizing solutal contribution; (c) $R_S = -10$, a stabilizing solutal contribution.

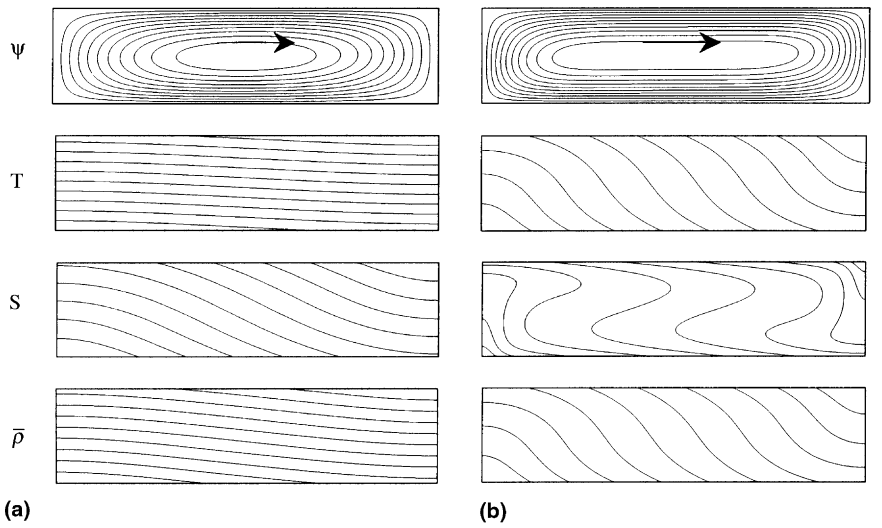

Fig. 3. Contour lines of stream function Ψ, temperature T, concentration S and density $\bar{\rho} = -(T + NS)$ for $R_S = 10,\ Le = 10,\ A = 4$: (a) $R_T = 5$, (b) $R_T = 25$.

tion fields to the buoyancy forces are of the same order. As the value of R_T is made larger than the pure thermal threshold, the resulting flow becomes much stronger, as illustrated in Fig. 3(b) for $R_T = 25$. In this flow regime, driven by the temperature gradients, the concentration field in the central part of the cavity is almost uniform. This is due to the large mixing resulting from the strong convective motion induced by the thermal-dominated regime.

The case $R_S = -10$ for which a stabilizing solutal influence competes with a destabilizing thermal influence is depicted in Fig. 2(c). The resulting diagram indicates the occurrence of a subcritical bifurcation characterized by the fact that the onset of motion occurs through nonlinear instabilities. This type of bifurcation is possible only when the two buoyancy forces are opposing each other and when the stabilizing agent is the slower diffusion component ($Le > 1$). For this situation, the solutal branches depicted as dashed lines are now unstable. They are connected with the stable thermal branches, depicted as solid lines, by saddle-node bifurcations.

5.2. Convection in the presence of side heating ($a \neq 0$)

In this section the effects of side heating intensity a, on the bifurcation curves discussed in the above section, are investigated. Figs. 4(a) and (b) show the analytical solutions predicted by the parallel flow approximation for the case $Le = 10$ and $R_S = 20$ and -20, respectively. The solutions have the form of the curved surfaces in a

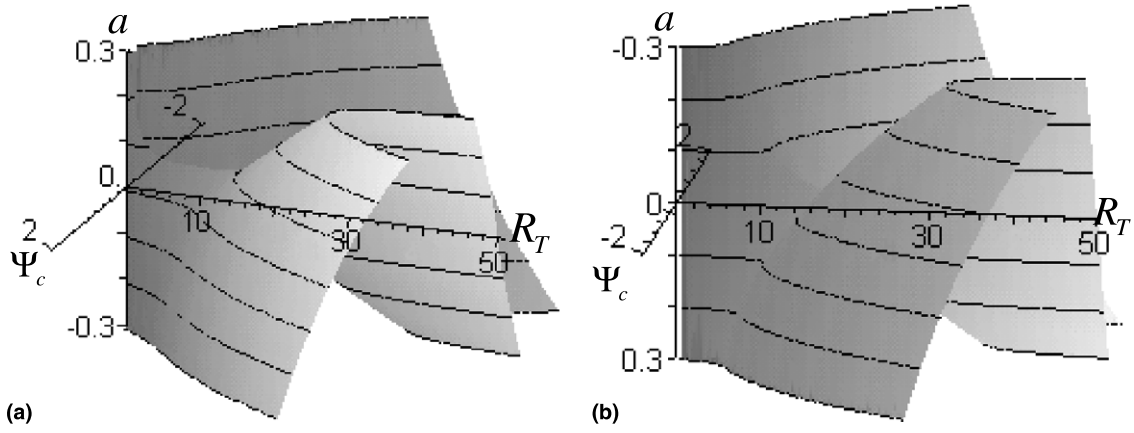

Fig. 4. Solution surface showing Ψ_c as a function of R_T and a for $Le = 10$ and (a) $R_S = 20$, (b) $R_S = -20$.

three-dimensional space with Ψ_c given as a function of R_T and a. An equivalent result was obtained by Kalla et al. [17] for the case of a porous cavity subject to uniform heat fluxes on all sides. For $a = 0$, the solution corresponds to the intersection between the curved surface and the plane $a = 0$ and takes the form of a standard Bénard bifurcation (see Fig. 2). On the other hand, for $a \neq 0$ the side heating acts as an imperfection brought to the bifurcation curves. Another type of imperfection has been considered in the past by Sen et al. [18] while investigating the effect of small tilt angles about the horizontal position on natural convection in a porous layer heated from the bottom.

Fig. 5 shows the effect of side heating ($a = 0.1$) on the magnitude of the stream function at the centre of the cavity Ψ_c as a function of R_T for $Le = 10$ and $R_S = 20$.

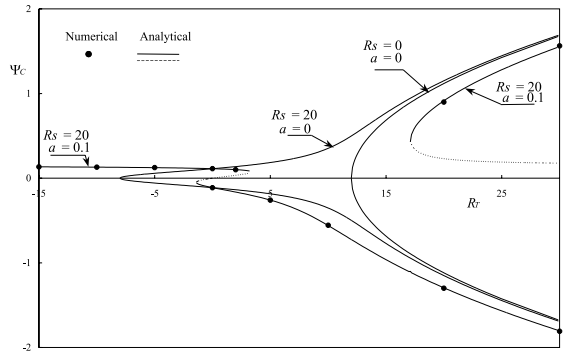

Fig. 5. Flow intensity Ψ_c as a function of R_T for $R_S = 20$, $Le = 10$ and side heating with $a = 0$ and 0.1.

The analytical solution, predicted by the present theory, is represented by the solid (stable) and dashed (unstable) lines and is seen to be in good agreement with the numerical results depicted by blackened circles. For comparison, the bifurcation curves corresponding to convection in the absence of side heating ($R_S = 20$, $a = 0$) and for pure thermal situation ($R_S = 0$, $a = 0$) are also included in the graph.

As it can be seen from Fig. 5, convection in the presence of side heating ($a \neq 0$) is possible for any value of the thermal Rayleigh number R_T. The case $R_T = 0$ will be considered first. This situation corresponds to the case of a layer salted from below. Since the solutal Rayleigh number $R_S = 20$ is above the value of the supercritical Rayleigh number $R_{Sc}^{sup} = 12$, convection occurs. The resulting cell can rotate indifferently clockwise or counterclockwise, giving rise to two different convection states. The transition from these two solutions, in the vicinity of $R_T = 0$, will be discussed latter. The case $R_T < 0$ corresponds to the situation where the direction of the heat fluxes depicted in Fig. 1 is reversed. Thus, the thermal contribution applied on the bottom of the cavity is now stabilizing while the right and left vertical walls are heated and cooled, respectively. As a result the fluid flows up along the right heated wall and comes down the left cooled wall giving rise to a counterclockwise cell and a positive value of Ψ_c. Naturally, for $R_T > 0$ the flow circulation is clockwise, in agreement with the thermal boundary conditions of Fig. 1, with a negative value of Ψ_c. These flows, which numerically can develop from rest as initial conditions are referred as "natural" flows (see for instance [18]). However, Fig. 5 indicates that, as the magnitude of R_T is

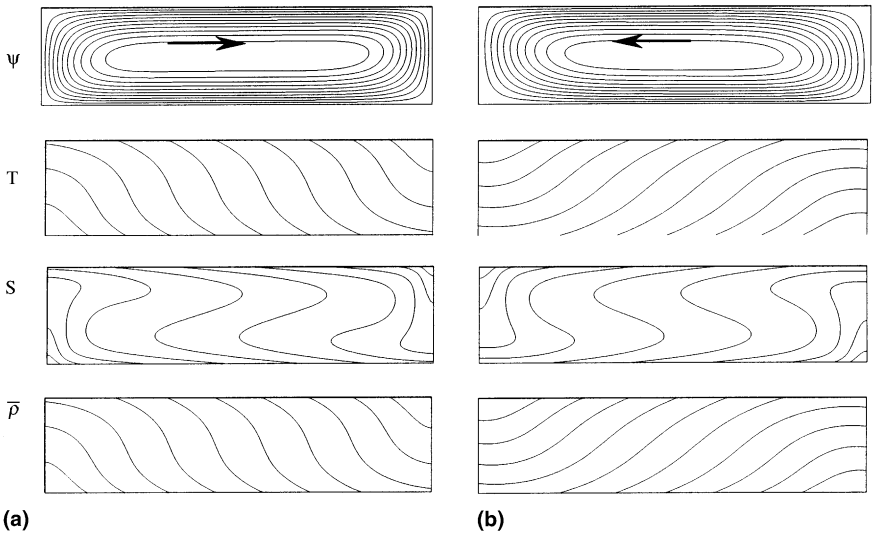

Fig. 6. Contour lines of stream function Ψ (top), temperature T, concentration S and density $\bar{\rho} = -(T + NS)$ for $R_T = 25$, $R_S = 20$, $Le = 10$, $A = 4$ and $a = 0.1$: (a) natural solution and (b) antinatural solution.

increased above a critical Rayleigh number $R^a_{Tc} \approx 17$, the value of which depends on R_S, Le, and a, other solutions corresponding to counterclockwise circulations are possible. These flows, which circulate in a direction opposite to that discussed above are called "antinatural". These two types of solutions are illustrated in Figs. 6(a) and (b) which show the contour lines of streamfunction, temperature, concentration and normalized density for the natural and the antinatural stable flows that coexist for $R_T = 25, R_S = 20, Le = 10, a = 0.1$ and $A = 4$. Also the curve corresponding to natural (counterclockwise flow) solution for $R_T < 0$ becomes antinatural for $0 < R_T \leqslant 6$. As observed from Fig. 5, the antinatural analytical solution for $R_T \geqslant 17$ consists of two branches, one stable, indicated by a solid line, the other one unstable, by a dashed line. Numerical confirmation of the stable antinatural states can be reached upon only using an impulsive flow pattern rotating in the appropriate direction as an initial condition. Once an antinatural state could have been obtained, for a given value of R_T, it can be used as initial conditions to run another antinatural state for new R_T. Since small differences in R_T are required to assure convergence the procedure may become prohibitively time-consuming to check a complete branch, especially near the turning point. On the other hand, it has not been possible to obtain numerical confirmation of the unstable branch of the antinatural analytical solution, and this, independently of the initial conditions used to initiate the numerical runs.

The existence of multiple solutions in the vicinity of $a = 0$ will be now discussed. The solution surface drawn in Fig. 4(a) may also be cut by Ψ_c–a planes located at different R_T, resulting in contour lines of the type shown in Figs. 7(a)–(c) for the case $R_S = 20$ and $Le = 10$. In the absence of the side heating ($a = 0$), according to the linear stability theory, Eq. (33), for $R_S = 20$ convection is possible only when $R_T \geqslant -8$. Fig. 7(b) shows the bifurcation curve obtained for $R_T = -8$. For this situation, when $a = 0$, the value of Ψ_c is also zero since R_T corresponds exactly to the critical Rayleigh number for the onset of motion. The effect of the side heating is to induce a natural convective cell, the intensity of which increases with the magnitude of a. Figs. 7(a) and (c) show the results obtained for $R_T > -8$. For this situation, it is observed that multiple solutions (stable and unstable) are possible in the vicinity of $a = 0$. Fig. 7(a) shows the results obtained for $R_T < 0$, namely $R_T = -2$. The case $a = 0$ corresponds to a pure Bénard situation and the flow can rotate indifferently clockwise and counterclockwise. For $a > 0$, the curves above and below the abscissa correspond to natural and antinatural states, respectively, and the converse is true for $a < 0$. Fig. 7(c) shows the results obtained for $R_T > 0$, namely $R_T = 10$. The resulting bifurcation diagram is seen to be qualitatively the mirror-image of the case with R_T negative (see for instance Fig. 7(a)). It is noticed that for a given R_T, there is a critical value of a for the existence of an antinatural state. Here again a good agreement is obtained between the analytical and the numerical results.

Figs. 8(a)–(c) show the effect of side heating a on the magnitude of the stream function at the center of the cavity Ψ_c, Nusselt number Nu and Sherwood number Sh as a function of R_T for $Le = 5$ and $R_S = -20$. A good agreement between the analytical

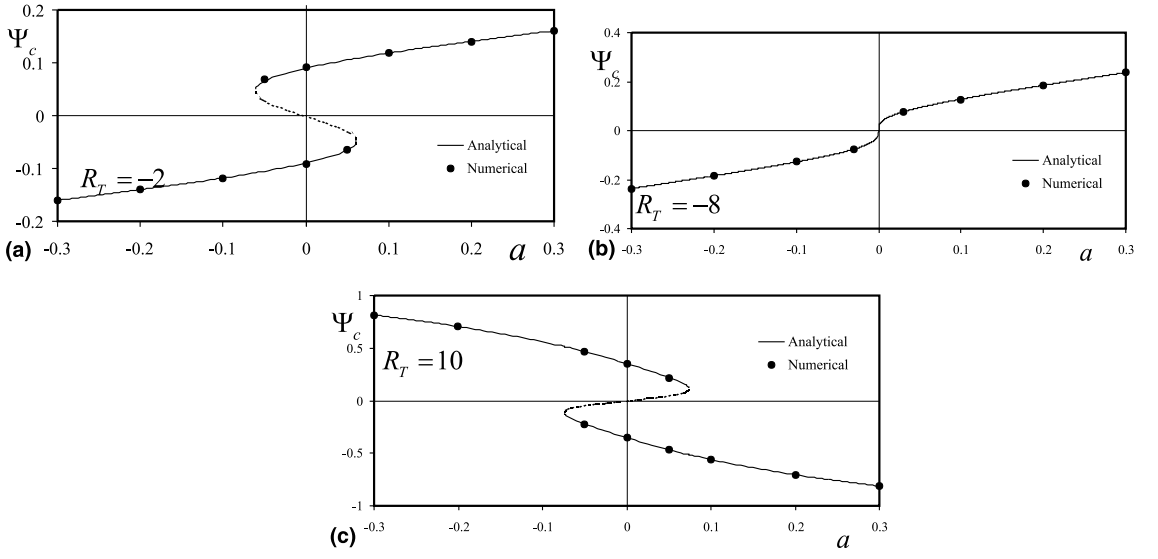

Fig. 7. Flow intensity Ψ_c as a function of a for $R_S = 20$, $Le = 10$: (a) $R_T = -2$, (b) $R_T = -8$ and (c) $R_T = 10$ (——— stable solution, - - - - unstable solution).

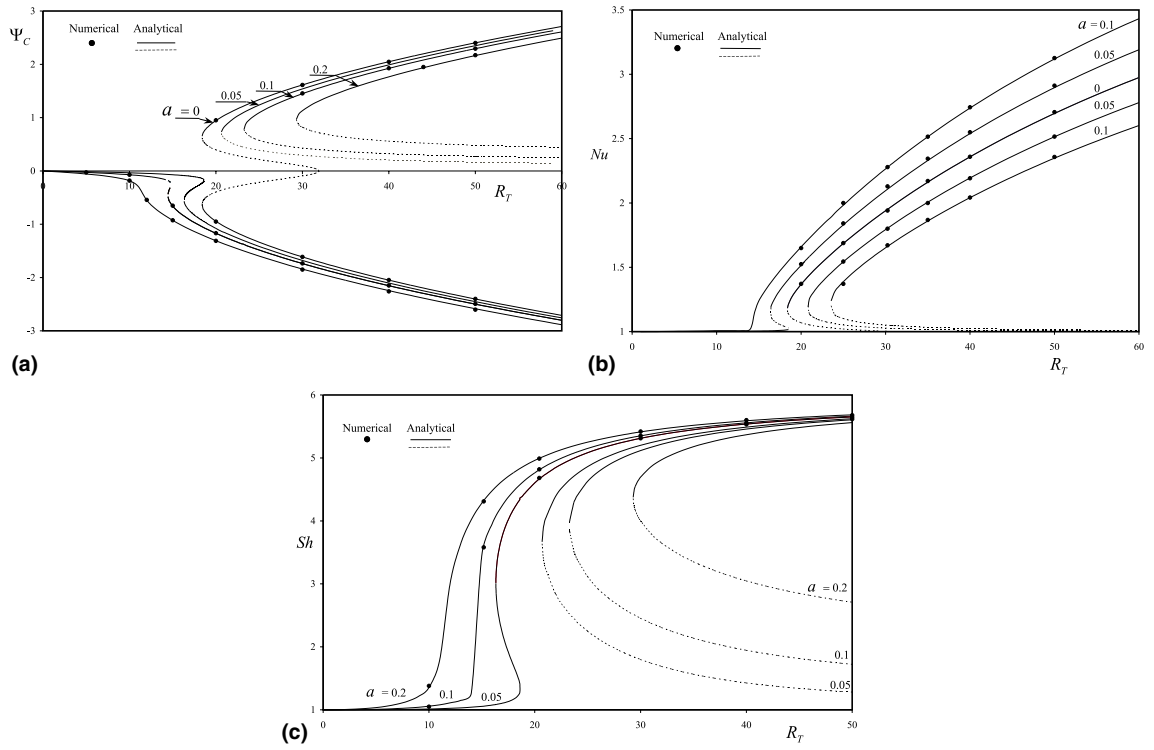

Fig. 8. Bifurcation curves as a function of R_T and a for $R_S = -20$ and $Le = 5$: (a) flow intensity Ψ_c, (b) Nusselt number Nu and (c) Sherwood number Sh (——— stable solutions, - - - - unstable solutions).

and the numerical results is observed in these graphs. In the absence of the side heating ($a = 0$), as already discussed in Fig. 2, the bifurcation curve is subcritical due to the fact that the buoyancy forces induced by the thermal and solutal contributions are opposing each other, the destabilizing agent being the faster diffusion component ($Le > 1$). Thus, convection is possible below the supercritical Rayleigh number $R_{Tc}^{sup} = 32$ down to the subcritical value $R_{Tc}^{sub} \approx 18.32$, as predicted by Eqs. (33) and (34) respectively. Upon applying side heating, it is seen from Fig. 8(a) that for a given a, three different convective states are possible for a given range of R_T; one of these solutions being unstable.

Finally it is noticed that if a is small enough the natural solution "penetrates" in the subcritical range $R_{Tc}^{sub} \leqslant R_T \leqslant R_{Tc}^{sup}$. Also, the existence of two antinatural convective states, one of which is unstable is also possible for the same range of R_T. Thus the analytical solution predicts the existence of five different solutions, two of which are unstable. This point is illustrated in Fig. 9, for the case $R_S = -20$, $Le = 10$ and $a = 0.005$. For this situation three stable solutions were obtained numerically for $R_T = 18$, as illustrated in Figs. 10 (a)–(c), one of the solutions being antinatural and the two others natural. Here again, appropriate initial conditions had to be used to simulate the two different antinatural

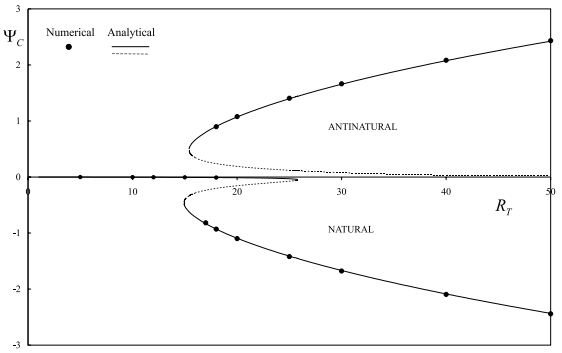

Fig. 9. Flow intensity Ψ_c as a function of R_T for $R_S = -20$, $Le = 10$ and $a = 0.005$.

solutions. As the intensity of the side heating is made larger, the penetration of the natural flow within the subcritical region disappears progressively and only two stable multiple convective states are possible for sufficiently high values of R_T.

6. Conclusions

The problem of thermosolutal convection in a shallow porous layer subject to cross fluxes of heat and mass

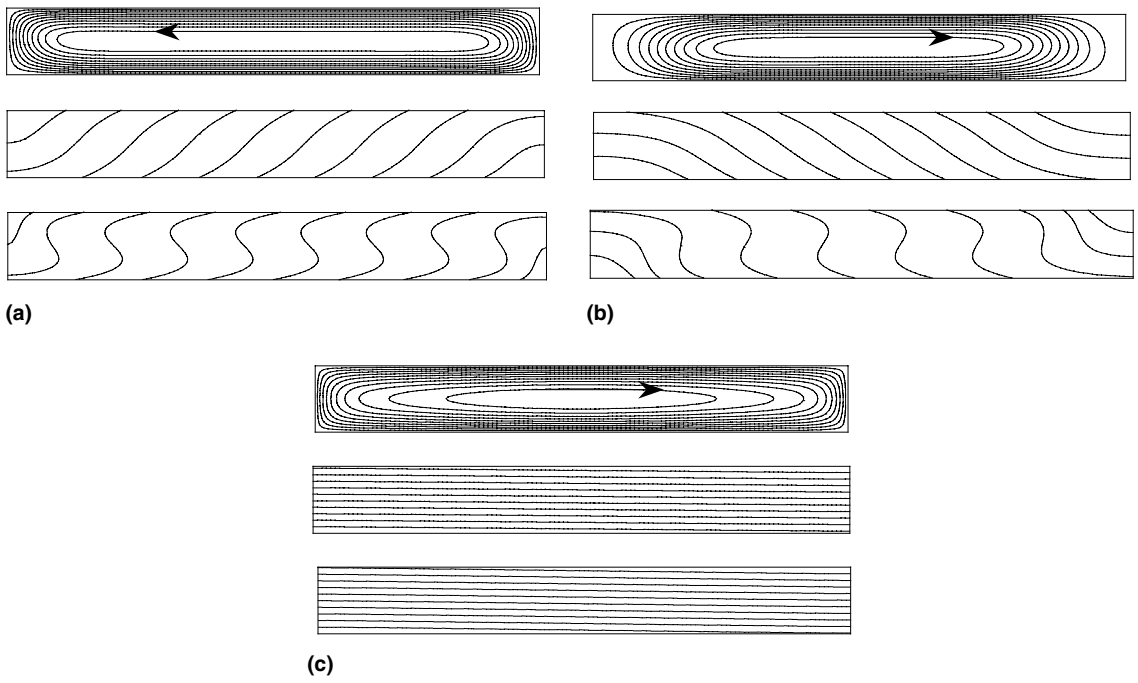

Fig. 10. Contour lines of stream function Ψ (top), temperature T and concentration S for the case $R_S = -20$, $R_T = 18$, $Le = 10$, $A = 8$ and $a = 0.005$: (a) natural solutions and (b) and (c) antinatural solutions.

has been investigated. Analytical solutions for the stream function, temperature and solutal fields, in the central region of the cavity, are obtained using a parallel flow approximation. The analytical results indicate that for supercritical convection, when both the solutal and thermal contributions are destabilizing, up to three different solutions, one of these solutions being unstable, are possible for a given set of the governing parameters provided that R_T is made higher than a critical value which depends upon R_S, Le and a. On the other hand, for subcritical convection which occurs when the two buoyancy forces are opposing each other and when the stabilizing agent is the slower diffusion component, up to five different solutions (two of which are unstable) are possible. The existence of multiple solutions in the vicinity of $R_T = 0$ has also been demonstrated.

A finite difference method is used to obtain numerical solutions of the full governing equations. A good agreement is observed between the analytical predictions and the numerical simulations.

Acknowledgements

This work was supported in part by the Natural Sciences and Engineering Research Council, Canada and jointly by FCAR, Government of Quebec.

References

[1] D.A. Nield, A. Bejan, Convection in Porous Media, 2nd ed., Springer, Berlin, 1998.
[2] D.A. Nield, Onset of thermohaline convection in porous medium, Water Resour. Res. 4 (1968) 553–560.
[3] J. Taunton, E. Lightfoot, T. Green, Thermohaline instability and salt fingers in a porous medium, Phys. Fluids 15 (1972) 748–753.
[4] H.Y. Rubin, Effect of solute dispersion on thermal convection in a porous medium layer, Water Resour. 9 (1973) 968–974.
[5] N. Rudraiah, P.K. Shrimani, R. Friedrich, Finite amplitude convection in a two-component fluid saturated porous layer, Int. J. Heat Mass Transfer 25 (1982) 715–722.
[6] D. Poulikakos, Double diffusive convection in a horizontal sparsely packed porous layer, Int. Com. Heat Mass Transfer 13 (1986) 587–598.
[7] M. Taslim, U. Narussawa, Binary fluid composition and double diffusive convection in a porous medium, J. Heat Transfer 108 (1986) 221–224.
[8] M.S. Malashetty, Anisotropic thermoconvective effects on the onset of double diffusive convection in a porous medium, Int. J. Heat Mass Transfer 39 (1993) 2397–2401.
[9] H. Brand, V. Steinberg, Non-linear effect in the convective instability of a binary mixture in a porous medium near threshold, Phys. Lett. 93A (1983) 333–336.
[10] T.H. Nguyen, T.T. Ha, P. Vasseur, Onset and development of double diffusive convection in horizontal porous layer,

in: Proceeding of the International Conference on Engineering Mechanics today EMT'97, Hanoi, Vietnam, 1997.

[11] M. Mamou, P. Vasseur, E. Bilgen, D. Gobin, Double-diffusive convection in an inclined slot filled with porous medium, Eur. J. Mech., B/Fluids 14 (1995) 629–652.

[12] O.V. Trevisan, A. Bejan, Mass and heat transfer by high rayleigh number convection in a porous medium heated from below, Int. J. Heat Mass Transfer 30 (1987) 2341–2356.

[13] N.D. Rosenberg, F.J. Spera, Thermohaline convection in a porous medium heated from below, Int. J. Heat Mass Transfer 35 (1992) 1261–1272.

[14] F. Chen, C.F. Chen, Double-diffusive fingering convection in a porous medium, Int. J. Heat Mass Transfer 36 (1993) 793–807.

[15] O.V. Trevisan, A. Bejan, Mass and heat transfer by natural convection in a vertical slot filled with porous medium, Int. J. Heat Mass Transfer 29 (1986) 403–415.

[16] M. Mamou, P. Vasseur, Thermosolutal bifurcation phenomena in a porous enclosure subject to vertical temperature and concentration gradients, J. Fluid Mech. 395 (1999) 61–87.

[17] L. Kalla, M. Mamou, P. Vasseur, L. Robillard, Multiple steady states for natural convection in a shallow porous cavity subject to uniform heat fluxes, Int. Commun. Heat Mass Transfer 26 (6) (1999) 761–770.

[18] S. Mihir, P. Vasseur, L. Robillard, Multiple steady states for unicellular natural convection in an inclined porous layer, Int. J. Heat Mass Transfer 30 (10) (1987) 2097–2113.